Nanoscale Advances

ROYAL SOCIETY OF CHEMISTRY

PAPER

View Article Online
View Journal | View Issue

Check for updates

Cite this: *Nanoscale Adv.*, 2024, **6**, 5636

Impact of polymorphism *vs.* shape of titania nanocrystals on the hydrogen evolution reaction†

Ankur Yadav,[a] Vivek Kumar Agrahari,[a] Yuriy Pihosh,[b] Mamiko Nakabayashi,[c] Wojciech Nogala,[d] Balendu Sekhar Giri,[e] Kazunari Domen,[bg] Daya Shankar Pandey,*[a] Bhavana Gupta *[df] and Subha Sadhu *[a]

Received 10th June 2024
Accepted 1st September 2024

DOI: 10.1039/d4na00479e

rsc.li/nanoscale-advances

Herein, we investigated the impact of polymorphism *vs.* dimension control of titania nanocrystals towards hydrogen generation. Two different forms of titania nanoparticles have been synthesized following the solvothermal method, leading to the formation of two distinct physicochemical features. Detailed structural, morphological, and optical studies revealed that the formation of titania nanorods correspond to rutile while granular particles correspond to the anatase phase. Among various titania polymorphs, anatase is well known for its superior photocatalytic activity; however, to our surprise, the as-synthesized rutile nanorods exhibited higher catalytic activity in comparison to anatase spheres, and hydrogen evolution was considerably enhanced after the addition of a minute amount of Pt as the co-catalyst. Thus, despite the higher catalytic activity of anatase, the enhanced hydrogen evolution of rutile nanorods may be related to the creation of a 1D structure. Our study highlights the importance of considering not only TiO_2 polymorphism but also shape and dimension in optimizing photocatalytic H_2 production.

Introduction

Hydrogen fuel is one of the promising and reliable sources of green energy and can be photocatalytically produced from water utilizing solar light.[1,2] For the first time, Fujishima and Honda reported the formation of gaseous hydrogen (H_2) through photoelectrochemical (PEC) water splitting using titania (TiO_2) as the photoelectrode.[3] After this report, different research groups have extensively explored water splitting in the presence of diverse photoelectrodes.[4–6]

Over the last ten years, TiO_2 has been popular for PEC due to its stability, unique optoelectronic properties, and nontoxicity.[7–9] Owing to the difference in electronic structure, the physiochemical properties of titania largely depend on crystallinity, shape, and size.[10] Amongst the polymorphs of titania, *i.e.*, anatase, rutile, and brookite, the first two are most often used for water-splitting reactions as catalysts. Extensive studies on different polymorphs of titania demonstrated that anatase shows superior photocatalytic activity related to rutile.[11] Many factors, such as the stability of the compound in aqueous solution under UV irradiation, superior oxidizing and reducing properties, and the band gap of the material, significantly influence the photocatalytic performance.[12] The band gap of anatase (3.2 eV) exceeds that of rutile (3.0 eV), resulting in reduced photon absorption for water splitting. The enhanced photocatalytic activity and water-splitting efficiency of the anatase phase are attributed to the presence of the valence band maximum at a higher energy level with respect to the redox potential of the adsorbed molecules.[13,14] In addition, along with the direct band gap, anatase exhibits a lower indirect band gap, thus facilitating exciton generation. Semiconductors with an indirect band gap often have higher charge carrier lifetime, thus accelerating efficient water splitting.[15–17] Moreover, the charge transport properties vary in individual polymorphs as a consequence of different crystal structures.

In addition to polymorphism, the photocatalytic activity depends on the shape and size of the semiconductor material. One-dimensional (1D) structures with varying dimensionalities, such as nanorods, nanotubes, and nanowires, are appealing as photocatalysts owing to their anisotropy and the presence of less grain boundary, thus assisting efficient charge transport. It is well established that photogenerated electron transport and collection are more effectively achieved with nanorod and nanowire arrays.[18–23] The photocatalytic performance of mixed-

[a]*Department of Chemistry, Institute of Science, Banaras Hindu University, Varanasi, India. E-mail: subha@bhu.ac.in; dspbhu@bhu.ac.in*

[b]*Office of University Professors, The University of Tokyo, 7-3-1 Hongo, Bunkyo-ku, Tokyo 113-8656, Japan*

[c]*Institute of Engineering Innovation, School of Engineering, The University of Tokyo, 7-3-1 Hongo, Tokyo, 113-8656, Japan*

[d]*Institute of Physical Chemistry, Polish Academy of Sciences, Kasprzaka 44/52, 01-224 Warsaw, Poland. E-mail: bhavana.gupta@ddn.upes.ac.in*

[e]*Sustainability Cluster, School of Advanced Engineering, UPES, Dehradun, India*

[f]*Department of Chemistry, Cluster of Applied Sciences, School of Advanced Engineering, UPES, Dehradun, India*

[g]*Research Initiative for Supra-Materials (RISM), Shinshu University, 4-17-1 Wakasato, Nagano 380-8533, Japan*

† Electronic supplementary information (ESI) available. See DOI: https://doi.org/10.1039/d4na00479e

phase titania, including rutile and anatase nanotubes, nanorods, and nanosquares, was examined for solar hydrogen production. It was observed that titania nanotubes exhibited a two-fold enhancement in hydrogen production compared to nanosquares.[24] In a separate study, Murakami *et al.* synthesized decahedral anatase titania with particle sizes ranging from 25 to 60 nm and found that 40 nm particles demonstrated superior photocatalytic activity due to their optimally enhanced surface area and efficient separation of redox sites.[25] The thermodynamic stability of the anatase phase is higher when the particle size is less than 11 nm; however, for the rutile phase, the stability of the compound increases when the particle size is >35 nm. Particles with smaller sizes are known to absorb more visible light and have lower electron–hole recombination.[26]

The impact of size on photocatalytic hydrogen generation has been previously studied independently.[27,28] However, to the best of our knowledge, the combined influence of the polymorph of TiO_2 and shape has not been thoroughly investigated. Though extensive studies have revealed that anatase exhibits superior photocatalytic activity compared to the other phases, it is important to know the impact of shape over polymorphism. What will be the effect on the catalytic activity if 1D rutile nanocrystals are used instead of anatase? Does anatase still have higher photocatalytic activity? To find the answer, in this present report, we synthesized various shapes of titania polymorphs and investigated their photocatalytic activity towards hydrogen production. Anatase nanospheres and rutile nanorods were synthesized by the solvothermal method, and the resulting systems were thoroughly characterized for their effectiveness in the hydrogen evolution reaction (HER). Our findings revealed that rutile nanorods exhibited three times higher catalytic activity compared to anatase nanospheres, leading to greater hydrogen generation through photocatalysis. It is well established that pure titania struggles to generate hydrogen in aqueous systems; consequently, researchers often utilize sacrificial reagents or noble metals, such as gold, palladium, or platinum, as co-catalysts to facilitate hydrogen evolution.[12,29] In our study, we employed 0.1 wt% platinum as a co-catalyst and observed a significant enhancement in the photocatalytic hydrogen evolution rate in rutile titania, with a boost in production rate of 30 times compared to that in the absence of a co-catalyst. Our study highlights the importance of the comparative study of titania polymorphs and dimensions to optimize photocatalytic H_2 production.

Experimental

Synthesis

Titanium tetrachloride ($TiCl_4$) was procured from Merck India Ltd while potassium tetrachloroplatinate ($K_2[PtCl_6]$) and titanium butoxide $Ti(O\text{-}Bu)_4$ (purity 97%) were obtained from Aldrich. However, common solvents like ethanol, methanol, toluene and hydrochloric acid (HCl) were procured from Aldrich.

The synthesis procedure of two different shapes of TiO_2 nanoparticles is illustrated in Fig. 1. To synthesize TiO_2 nanorod, 5 mL toluene was taken in a clean Teflon cup, followed by the addition of 0.3 M titanium butoxide $Ti(O\text{-}Bu)_4$ and 1 M titanium tetrachloride ($TiCl_4$). After 30 min of stirring at room temperature, 0.5 mL of concentrated HCl was added to the solution. Moreover, the mixture was stirred for 30 min and the Teflon cup containing the mixture was kept in a steel autoclave and placed inside a muffle furnace at 180 °C for 9 h. After the completion of the reaction, the product in the form of a precipitate was collected, washed in ethanol, and centrifuged. After centrifugation, the precipitate was dried in an oven at 60 °C and the dried powder was used for additional characterization. Similarly, TiO_2 granular particles were synthesized using ethanol as a solvent instead of toluene, $Ti(O\text{-}Bu)_4$ as the precursor and oleic acid and oleyl amine as the capping agent. Note that 6 mL ethanol, 0.8 M $Ti(O\text{-}Bu)_4$, 4.2 M oleic acid, and 4.2 M oleyl amine was added in a Teflon cup to prepare the solution and the solution was stirred for 30 min. Then, the solution was maintained in an autoclave at 180 °C for 18 h. After the completion of the reaction, the product in the form of a precipitate was washed, centrifuged, and dried.

Characterization

The crystal structure of the as-synthesized TiO_2 was determined by X-ray diffraction (XRD) (Smart Lab., Rigaku, Japan), equipped with CuKα ($\lambda = 1.5406$ Å) irradiation source and operated at 45 kV and 200 mA. The step size was 0.02°. The Raman spectra were acquired using a LabRam HR evolution spectrometer (manufacturer: Horiba). The samples were excited by a 532 nm laser line (He–Ne laser) operating at a power of 30 mW, utilizing a grating with 600 groves per mm.

To study the morphology of TiO_2 nanoparticles, scanning electron microscopy (SEM) (SU8020. Hitachi, Japan) and transmission electron microscopy ((S)TEM, JEM-2800, JEOL, Japan) characterization were performed using a X-MAX 100 TLE SDD detector operating at 200 kV. High-resolution TEM (HR-TEM) images were analyzed in Gatan Digital Micrograph 2.3 software. The elemental composition maps were acquired within the 10 keV channel with a resolution of 0.64 nm per px and a dwell time of 8192 μs using the Bruker Xflash detector with 129 eV energy resolution. The optical properties of TiO_2 nanoparticles were studied by FTIR and UV-visible diffuse reflectance spectroscopy (UV-vis-DRS) using a PerkinElmer FTIR instrument and a V-670 instrument (Jasco, Japan), respectively.

The PEC properties of the TiO_2 thin films' photoelectrodes were investigated using a three-electrode system with the specimen, Ag/AgCl in a saturated aqueous KCl solution, and a Pt wire connected to a potentiostat (Autolab model) as the working, reference, and counter electrodes, respectively. TiO_2 thin films photoelectrodes were fabricated using TiO_2 dispersion in isopropanol (20 mg in 50 μL). This dispersion was cast on an exposed area of ITO control by scotch tape boundary. Note that 0.5 M Na_2SO_4 (pH 7) was used as an electrolyte. A Xenon lamp (lumen 200) of 25 percent intensity, shining 60 Lumen (40 mW cm^{-2}) of light on the electrode, was used as a light source. Each PEC measurement was performed under Ar ambience in a gas-tight cell with an optical window.

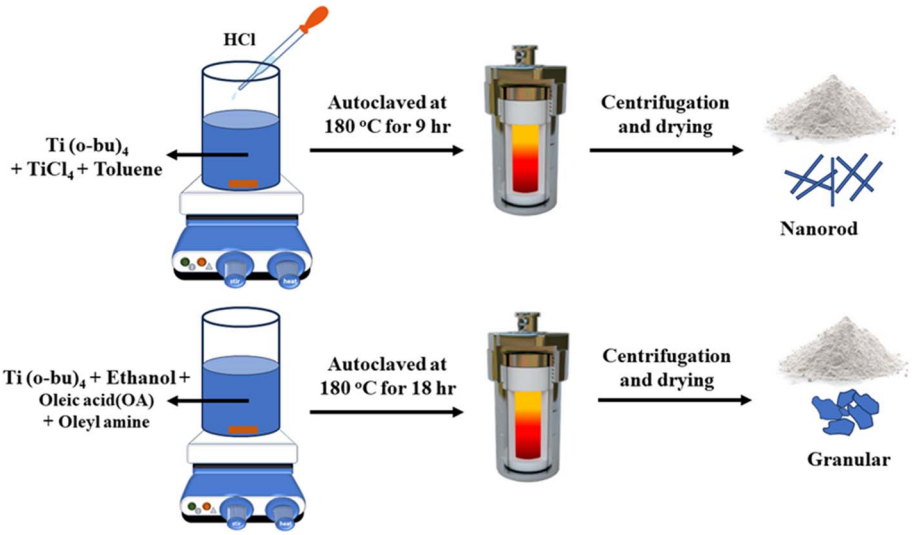

Fig. 1 Schematic of synthesis of TiO_2 nanoparticles in two different morphologies.

Photocatalytic H_2 generation

For the photocatalytic generation of hydrogen, 20 mg of TiO_2 powder was dispersed in a 40 mL mixture of methanol and water (with a ratio of 80 : 20) with and without the addition of 0.1% Pt. The addition of platinum was achieved *via* photodeposition. Specifically, 5 μL of a 20 mM K_2PtCl_6 solution was added to the TiO_2 dispersion in a methanol–water mixture, with a total volume of 40 mL, and a composition identical to that previously mentioned. The hydrogen gas generation was monitored until the deposition process was completed. The dispersion was achieved *via* sonication to ensure homogeneity. Subsequently, the prepared substances were placed in a Pyrex reactor, which was top-illuminated and connected to a closed gas circulation system. All photocatalytic reactions were conducted at 288 K under a background pressure of 5 kPa. To eliminate any air present in the reaction mixture, evacuation was carried out before introducing Ar gas to establish a background pressure of approximately 5 kPa. The reactant solution was then exposed to irradiation from a 300 W Xe lamp. The distance from the lamp to the sample was 10 cm. The gaseous products generated during these reactions were analyzed using an integrated online gas chromatography system. The system consisted of a chromatograph (GC-8A Shimadzu, Japan) equipped with molecular sieve having 5 angstrom columns and a thermal detector, with Ar serving as the carrier gas.

Results and discussion

The as-synthesized nanoparticles obtained by a solvothermal method that employed diverse solvents, precursors and capping agents are expected to have distinct phases and shapes. The difference in the shape and structural characteristics of the nanoparticles can considerably impact their optical and other physicochemical properties. XRD and Raman studies have been performed to verify the crystal structure and phase of the nanoparticles (Fig. 2a and b). The diffraction at angles of 25.3° and 27.5° were indexed for the anatase (101) and rutile (110) phase of TiO_2, respectively.[30,31] Moreover, the (101) and (211)

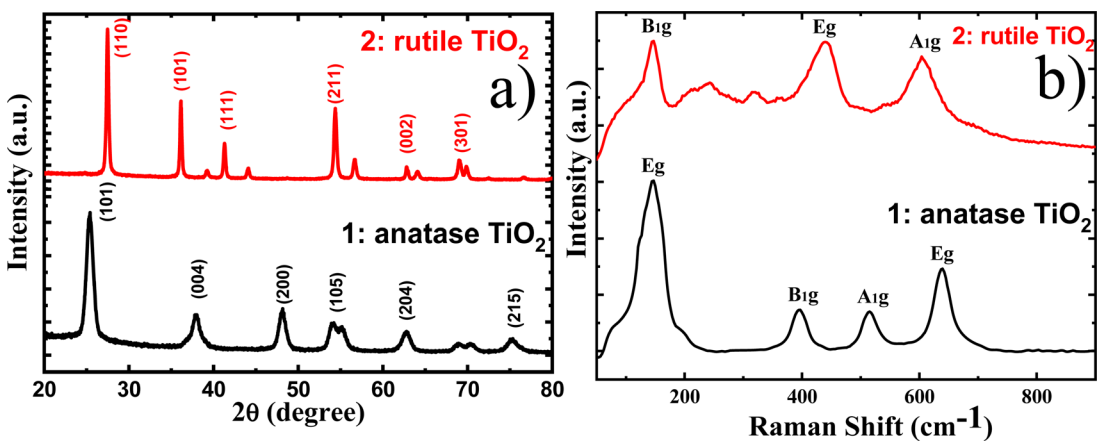

Fig. 2 (a) XRD pattern and (b) Raman spectra of anatase granular (1) and rutile TiO_2 nanorod (2).

diffraction planes of the rutile phase at 36.2° and 54.6° were observed, whereas the diffraction pattern at 48.1° and 54.9° corresponding to the (200) and (105) planes of anatase is detected.

It was observed that the XRD peak for anatase is broader than that for the rutile, which can be attributed to the smaller crystallite size of anatase. As the crystallite size decreases, the peaks in the XRD pattern tend to broaden. Fig. S1† shows the TEM images of the as-synthesized nanoparticles, revealing crystallite sizes of ~10 nm for anatase granular particles and 40 nm for rutile nanorods, thereby supporting the findings from XRD analysis. Due to its smaller crystallite size, anatase exhibits a higher surface area compared to rutile nanorods. The Brunauer–Emmett–Teller (BET) analysis indicates an observed surface area of 36.02 $m^2 g^{-1}$ for anatase and 14.76 $m^2 g^{-1}$ for rutile, as shown in Fig. S2.† Therefore, the as-synthesized anatase granular particles possess a greater surface area than the rutile nanorods. Rutile nanorods are synthesized in the presence of hydrochloric acid (HCl) and titanium precursors ($TiO(Bu)_4$ and $TiCl_4$), which exhibit differing rates of hydrolysis, with toluene serving as the solvent. A combination of different titanium precursors and was is introduced into the reaction vessel containing toluene to modulate the hydrolysis rate and facilitate the rapid precipitation of titanium hydroxides. The primary role of HCl is to regulate the hydrolysis rate, thus preventing the rapid precipitation of titanium hydroxide. The hydrolyzed precursors considerably influence the growth and morphology of the resulting nanocrystals.[28,29]

As the temperature increases, H^+ ions are released from the hydrolyzed precursor, leading to the formation of hydrated titanyl ions through intramolecular oxolation. Subsequently, with the further elevation of temperature and pressure within the hydrothermal reactor, condensation of the hydrated titanyl ions occurs, resulting in the formation of TiO_6 octahedra through the edge-sharing of hydrated titanyl ions in the equatorial position.[32] Thereafter, rutile nanorods are formed through the polymerization of octahedra, crystallizing into a one-dimensional structure along the *c*-axis. Previous studies have shown that when only $TiCl_4$ is utilized as a precursor, faceted truncated bipyramidal nanocrystals are obtained. Conversely, the exclusive use of $Ti(OBu)_4$ leads to the formation of an agglomerated film.[33] Therefore, both $TiCl_4$ and $Ti(OBu)_4$ precursors are essential for the successful formation of rutile nanorods.

The formation and purity of the anatase and rutile phase nanocrystals were confirmed through X-ray diffraction (XRD) analysis, which indicated the absence of additional peaks corresponding to impurities. Granular anatase nanocrystals are generated in the presence of capping agents, specifically oleic acid and oleylamine, which bind to high-energy facets during nucleation and facilitate the formation of granular nanoparticles.[34,35] Previous reports indicated that oleic acid and oleylamine exhibit differing binding strengths: oleic acid binds more strongly to the {001} facets of anatase, while oleylamine preferentially attaches to the {101} facets. This selective binding suppresses growth in the corresponding directions, thereby promoting the formation of nanospheres.[36] The formation and purity of the anatase and rutile phase nanocrystals were affirmed by XRD analysis, which clearly showed the absence of additional peaks due to impurity. Granular anatase nanocrystals are formed in the presence of capping agents (oleic acid and oleyl amine), which are used to attach to the high-energy facets during nucleation and promote the formation of granular nanoparticles.[34,35] Hence, the selective binding hinders the growth in the corresponding direction and aids in the formation of nanospheres.[36]

The formation of pure phase anatase and rutile nanoparticles has been confirmed by Raman analyses (Fig. 2b). The granular anatase nanoparticles displayed characteristic peaks at 144, 396, 515 and 637 cm^{-1} corresponding to E_g, $B1_g$, $A1_g$ and E_g vibration modes. Conversely, rutile nanorods exhibited characteristic Raman active fundamental vibration at 439 and 606 cm^{-1} corresponding to the E_g and $A1_g$ mode, respectively, along with second-order vibration at 146 cm^{-1}. The E_g and A_{1g} vibration modes are caused by the asymmetric bending and symmetric stretching of the O–Ti–O bond along the {001} and {110} planes, respectively.[37]

FTIR spectra provided additional structural information of the nanoparticles (Fig. S3†). The crystallinity of the material can be correlated with the peak intensity between 750 and 1000 cm^{-1}, with the anatase exhibiting greater intensity related to the rutile phase, probably due to the nanocrystallization/defect centre during hydrothermal synthesis.[38]

Following the confirmation of the formation of pure anatase and rutile nanoparticles, our research aimed to investigate the optical properties and band structure of the as-synthesized compounds as the band gap of these materials plays a crucial role in H_2 generation.[29,39,40] The band gap was determined from UV-vis-DRS spectra using Kubelka–Munk's function (Fig. 3), revealing values of 3.2 eV for anatase and 3 eV for rutile. The sharp transition observed near the band edge is attributed to the electronic transition from the valence band of O_{2p} to the conduction band of Ti_{3d}. Interestingly, the rutile phase exhibited a 0.2 eV lower band gap compared to the anatase phase, in line with an earlier report.[41]

It is hypothesized that the low band gap observed in the rutile phase TiO_2 is due to a downward shift in the conduction

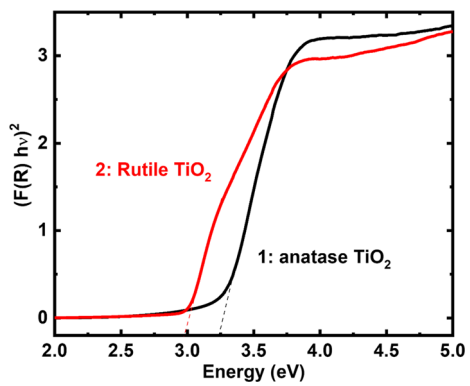

Fig. 3 Band gap determination of as-synthesized anatase granular (1) and rutile TiO_2 nanorod (2) from UV-vis-DRS spectra using Kubelka Munk function.

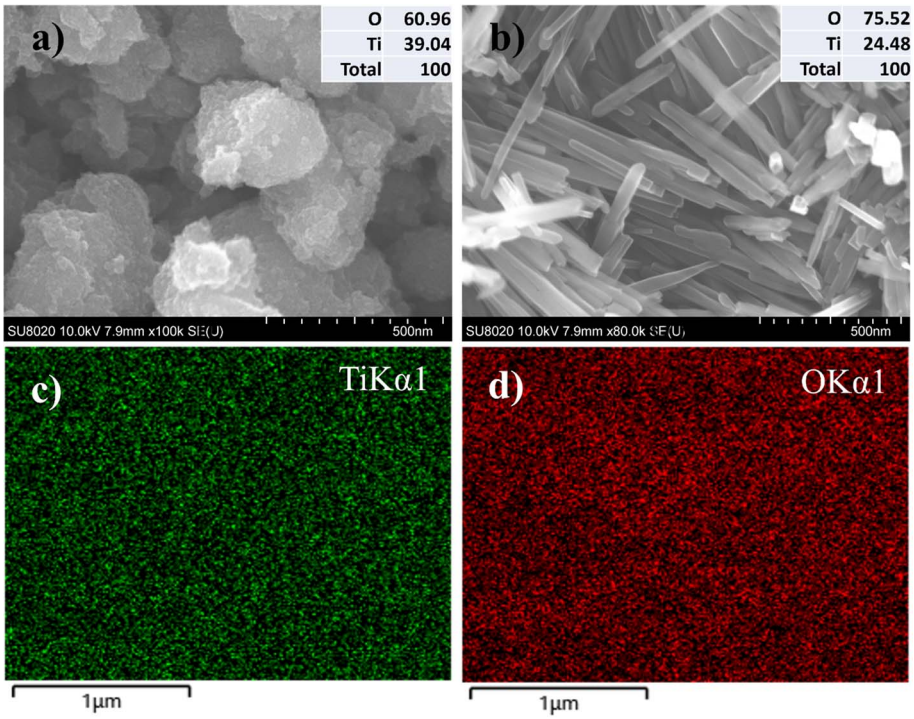

Fig. 4 SEM images of (a) anatase granule and (b) rutile TiO_2 nanorod (inset-atomic percentage of Ti and O). (c) Ti and (d) O mapping of the TiO_2 nanorod surface.

band energy. Enhanced H_2 generation is most effectively achieved with a low band gap; however, the catalytic performance is also influenced by other physicochemical characteristics. Therefore, a comprehensive study of the surface properties, morphology, and photoelectrochemical characteristics is essential before investigating the photocatalytic H_2 evolution feature.

The crystalline phase and shape of TiO_2 can be controlled by the choice of solvent, precursor, and capping agent. Fig. 4a and b illustrate that the use of a capping agent in ethanol yields granular anatase TiO_2 nanoparticles, while TiO_2 nanorods are obtained without a capping agent in toluene. Energy-dispersive X-ray (EDAX) spectroscopy mapping reveals a uniform distribution of titanium (Ti) and oxygen (O) across the surface, along with the calculation of the atomic weight percentages of these elements (see Fig. 4c, d and ESI Fig. S4†) Notably, the solvent used in the synthesis influences the nanoparticles' morphology and surface properties and impacts the O/Ti ratio, as shown in Fig. 4a and b-inset. Rutile phase TiO_2 nanorods exhibit a higher O/Ti ratio compared to anatase phase TiO_2 spheres. The oxygen-to-titanium (O/Ti) ratios were also determined using X-ray photoelectron spectroscopy (XPS), yielding values 1 : 2.04 for anatase granular and 1 : 2.40 for rutile nanorods. These results are consistent with the trends observed in the EDAX analysis. The XPS spectra and the calculations of the O/Ti ratios are provided in the ESI (Fig. S5, S6, and Table S1†).

The resistivity of TiO_2 is strongly correlated with the ratio of O/Ti. The material's resistivity increases with a larger ratio and *vice versa*. Increased resistivity has an adverse effect on the electron transfer, or charge transfer, that occurs during photocatalysis.[42] However, because the path for charge transport is shorter in the nanostructure shape, photocatalysis benefits from shorter path length during photocatalysis.[43] The Ti and O ratios for TiO_2 rutile (nanorod) and TiO_2 anatase (granular) were found to differ based on the EDAX mapping. This difference in the ratio ultimately affects the overall electron transfer to the adjacent moiety in water (photocatalysis) or electrode (photoelectrocatalysis) and competes with the effect of path length.

Following particle transfer on an ITO surface at equal amounts and surface area, photoelectrochemical studies were conducted utilizing voltametric and impedance techniques (as depicted in Fig. 5a and b) to assess the charge transfer resistance.[44] Rutile TiO_2 exhibited approximately three times higher catalytic current under light irradiation compared to anatase TiO_2 using linear sweep voltammetry (LSV). Consistent results were observed in impedance measurements *via* the Nyquist plot, demonstrating a charge transfer resistance in rutile TiO_2 three orders of magnitude lower than in anatase TiO_2. A significant current was observed in the case of TiO_2 nanorods, likely due to efficient charge transfer from the materials to the electrode surface, facilitated by charge generation in the presence of light. The increased charge production can be attributed to the enhancement of diffusion length in the nanorods, which effectively compensates for the effects of charge recombination.

It can be inferred that the ratio of O/Ti plays a significant role in determining the resistivity of materials. Moreover, the morphology and band gap are important in influencing charge mobility and separation within the matrix. The results suggest

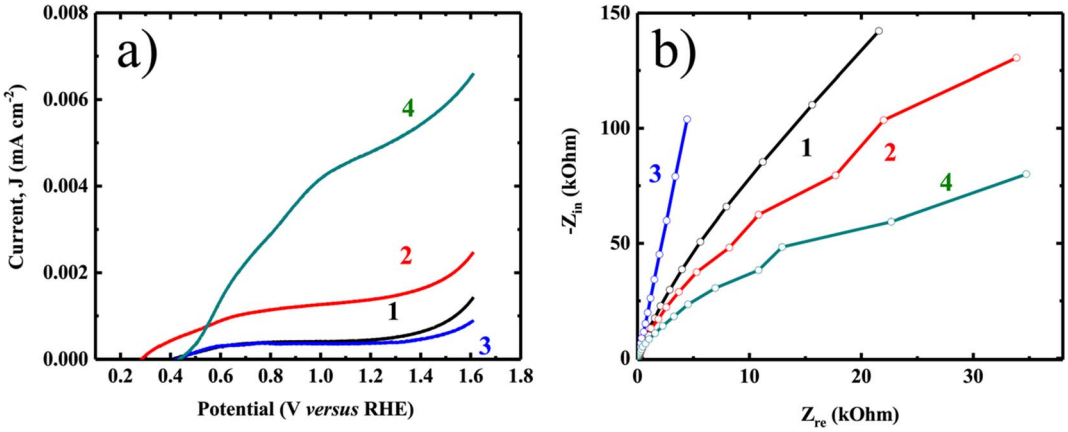

Fig. 5 (a) LSV and (b) Nyquist plot of anatase granular (1-dark 2-light) and rutile TiO_2 nanorod (3-dark 4-light).

that photocatalytic H_2 evolution will be much higher in the case of rutile TiO_2 compared to anatase TiO_2.

To evaluate the efficiency of photocatalytic H_2 generation and understand the influence of various physicochemical parameters, the as-synthesized TiO_2 nanoparticles with different morphology were further examined. The results depicted in Fig. 6a reveal that the TiO_2 nanorod morphology exhibited a higher rate of H_2 generation (average 1.2 μmol h^{-1} and highest 3 μmol h^{-1}) compared to the TiO_2 granular morphology (average 0.8 μmol h^{-1} and highest 1 μmol h^{-1}). The sustained stability of the nanorod during four hours of hydrogen production is evidence of the consistent rate of hydrogen evolution observed over three consecutive cycles (Fig. 6b and ESI Fig. S7†). This enhanced performance can be attributed to the superior dispersion of the nanorods due to their smaller size, which facilitates efficient light absorption and charge separation (Fig. S8a–c†). Thus, the size and dimensions of TiO_2 play a significant role in enhancing H_2 production. The morphology of TiO_2 nanorods aids in the efficient separation of light-generated charges due to their shorter surface diffusion length. Previous studies have indicated that various physicochemical properties affect the generation of H_2 on TiO_2 surfaces, with shape and size emerging as key factors in this process.[29,39]

As evidenced from the results above, the nanorod morphology of TiO_2 is beneficial for improving charge separation, a process that can be further optimized through the inclusion of a surface co-catalyst layer. TiO_2 nanorods were modified with 0.1 wt% of Pt to enhance charge separation during hydrogen production. The simultaneous deposition of Pt (in the form of nanoparticles) during hydrogen production eventually reached a plateau at 90 μmol h^{-1}, which was the highest rate of H_2 generation, while the average rate was 50 μmol h^{-1} once Pt deposition was complete. This suggests that the co-catalytic effect of charge transfer from the TiO_2 surface is enhanced in the presence of Pt nanoparticles, as illustrated in Fig. S8d.†

Fig. 7a displays the low-resolution TEM image of the TiO_2 rutile sample with Pt deposited on TiO_2 nanorod. The distribution of Pt partly (less than 10%) covers the TiO_2 nanorod surface (ESI S9†). This clearly supports the increase in the H2 evolution with increasing amount of Pt from 0.1 wt% to 1 wt%. Lattice fringes with interplanar distances of ~0.32 nm corresponding the (110) plane are observed in Fig. 7b, consistent

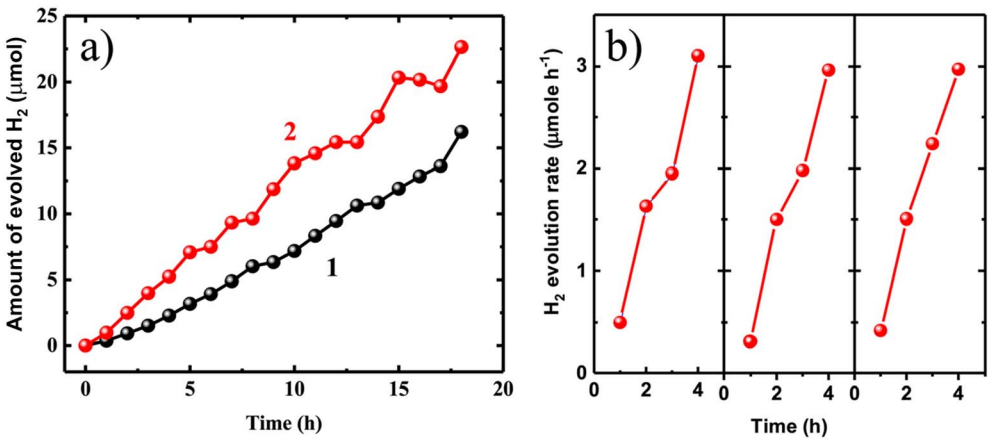

Fig. 6 (a) Photocatalytic H_2 generation under 300 W Xe-lamp for (1) anatase granular and (2) rutile TiO_2 nanorod, (b) three consecutive runs until maximum rate of H_2 generation.

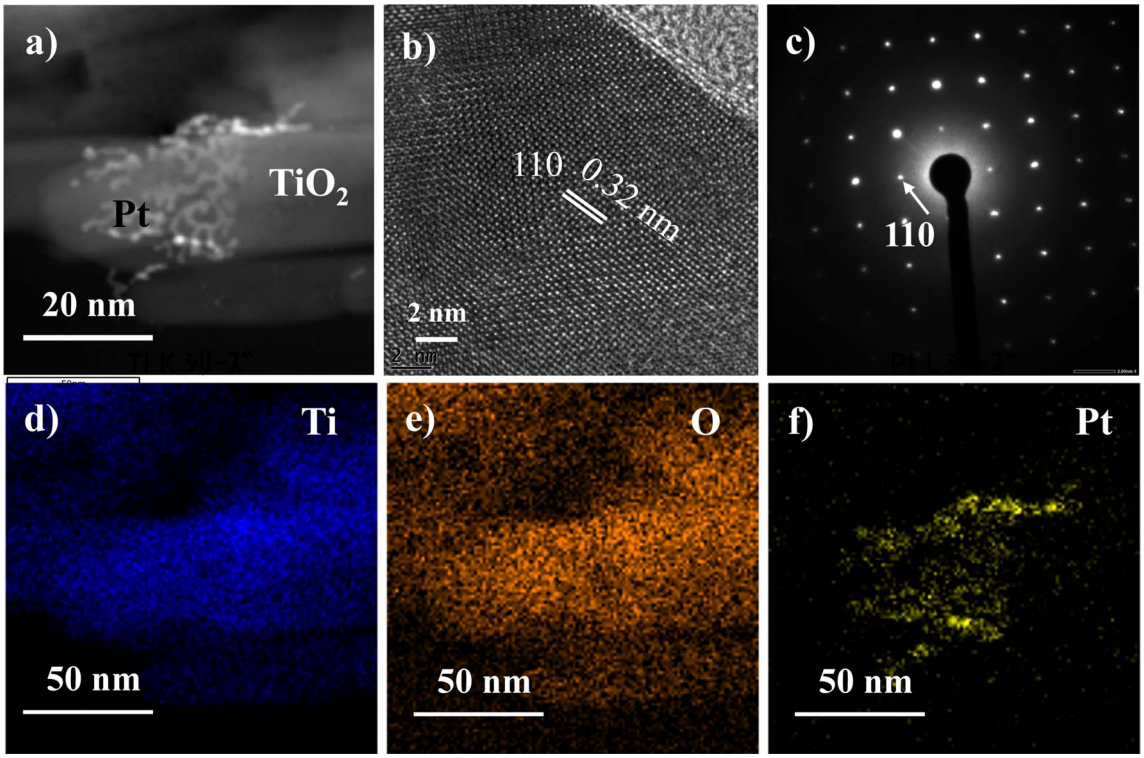

Fig. 7 (a) ADF STEM image of rutile TiO_2 nanorod after Pt deposition. (b) HRTEM image taken on the surface of rutile TiO_2 particle (c) SAED pattern for the rutile TiO_2 particle, confirming the formation of a single crystal and (d–f) elemental mapping for Ti, O, and Pt, respectively.

with the literature values.[45] The sharp and ordered selected area electron diffraction (SAED) pattern in Fig. 7c along the [001] zone axis confirms the single crystalline nature of the rutile nanorods. High-resolution TEM reveals the uniform deposition of 2–4 nm Pt nanoparticles in small patches on the surface of TiO_2 nanorod, as depicted in Fig. 7a. Elemental mapping in Fig. 7d–f further verifies the distribution of Pt on the nanorod surface. The nanorod structure provides a larger surface area for a precise and thin layer of Pt deposition, preventing agglomeration and significantly enhancing H_2 generation. The morphological characterization of the nanorods was performed after hydrogen evolution experiment (Fig. S9 and S10†), and no

Table 1 A summary of the key findings of Pt-doped TiO_2 photocatalysts reported in recent years for H_2 production

Pt loading on TiO_2	Light source	Crystalline phase of TiO_2	Photocatalyst loading (mg)	H_2 production efficiency	Quantum efficiency	Reference
Pt-5 wt%	500 W Hg–Xe lamp with dichroic filter (280–400 nm)	Anatase-rutile bulk	500 mg in 1 L in 1 : 9 MeOH/H_2O medium	27.6 mmol g^{-1} h^{-1}	5.6%	46
Pt-2.5 wt%	Black light blue lamp of 15 W	Anatase-rutile bulk	150 mg in 1 L containing 2 vol% ethanol	383 mmol h^{-1} g^{-1}	7.8%	47
Pt-1.0 wt%	300 W Xe lamp	Anatase nanosheet	5 mg in 100 mL water containing 10% methanol	5086 μmol h^{-1} g^{-1}	—	48
Pt-1.0 wt%	8 Philips CLEO 15 W	Anatase-rutile bulk	200 mg in 200 mL water containing 25 vol% methanol	1846 μmol h^{-1}	—	49
Pt-0.1 wt%	300 W Xenon lamp	Rutile nanorod	20 mg in 40 mL water containing 10 vol% methanol	Average 50 μmol h^{-1}, highest 90 μmol h^{-1}	Average 7.41%, highest 10.11%	Current work
Pt-1 wt%	300 W Xenon lamp	Rutile nanorod	20 mg in 40 mL water containing 10 vol% methanol	Average 150 μmol h^{-1}, highest 250 μmol h^{-1}	Average 22.23%, highest 30.33%	Current work

observable changes in the shape were detected. This indicates that the nanorods exhibit high photocatalytic stability.

Since the influence of Pt on H_2 generation is already well established in the literature, our result is compared with previous studies and illustrated in Table 1. The table demonstrates that the unique nanorod morphology facilitates cocatalyst deposition for enhanced H_2 production using minimal Pt, in contrast to prior studies requiring larger amounts of Pt. This effect is observed even in the less favorable rutile phase of TiO_2.

Conclusion

In summary, this study underscores the significance of TiO_2 morphology and crystalline phase in photocatalytic water reduction. Notably, the results suggest that the charge carrier diffusion path plays a crucial role, and nanorods exhibit a distinct advantage due to their one-dimensional shape. Specifically, the experiments show a threefold increase in H_2 generation (3 μmol h^{-1}) in rutile nanorods compared to anatase nanosphere (1 μmol h^{-1}), suggesting that the 1D structure is more effective for hydrogen production. The enhanced photocatalytic activity in TiO_2 nanorods is attributed to improved charge mobility. Therefore, the charge mobilities and exciton lifetime of the photocatalyst should be considered when optimizing the photocatalytic properties. Additionally, the uniform deposition of Pt cocatalyst on the nanorod surface further enhances charge carrier mobility, resulting in a 30–40-fold increase in H_2 gas evolution (average 50 μmol h^{-1} and highest 90 μmol h^{-1}). This study paves the way for future research to explore the impact of nano dimensions on the photocatalytic performance of the most effective photocatalyst.

Data availability

Data will be made available on request.

Conflicts of interest

There are no conflicts to declare.

Acknowledgements

B. G. acknowledges funding from the European Union's Horizon 2020 research and innovation programme under the Marie Skłodowska-Curie Grant Agreement No. 847413. Scientific work published as part of an international cofinanced project funded from the programme of the Minister of Science and Higher Education entitled "PMW" in the years 2020–2024; Agreement No. 5005/H2020-MSCA-COFUND/2019/2. This work was partially supported by "Advanced Research Infrastructure for Materials and Nano-technology in Japan (ARIM)" of the Ministry of Education, Culture, Sports, Science and Technology (MEXT), Grant Number JPMXP1223UT0004. This research was funded in part by the National Science Centre, Poland, through grant 2022/46/E/ST4/00457. S. S. acknowledges the financial support by the Department of Science and Technology, Government of India, under the DST Inspire Faculty Award (DST/INSPIRE/04/2021/000742). A. Y. and V. K. A. acknowledge the support from UGC for junior research fellowship.

References

1 Q. Hassan, S. Algburi, A. Z. Sameen, H. M. Salman and M. Jaszczur, Green hydrogen: A pathway to a sustainable energy future, *Int. J. Hydrogen Energy*, 2024, **50**, 310–333.
2 K. K. Jaiswal, C. R. Chowdhury, D. Yadav, R. Verma, S. Dutta, K. S. Jaiswal, B. Sangme and K. S. K. Karuppasamy, Renewable and sustainable clean energy development and impact on social, economic, and environmental health, *Energy Nexus*, 2022, **7**, 100118.
3 K. Maeda, Photocatalytic water splitting using semiconductor particles: History and recent developments, *J. Photochem. Photobiol., C*, 2011, **12**, 237–268.
4 B. Gupta, A. A. Melvin, T. Matthews, S. Dash and A. K. Tyagi, TiO_2 modification by gold (Au) for photocatalytic hydrogen (H_2) production, *Renewable Sustainable Energy Rev.*, 2016, **58**, 1366–1375.
5 B. Gupta, A. A. Melvin, T. Matthews, S. Dhara, S. Dash and A. K. Tyagi, Facile gamma radiolytic methodology for TiO_2-rGO synthesis: Effect on photo-catalytic H_2 evolution, *Int. J. Hydrog. Energy*, 2015, **40**, 5815–5823.
6 G. Liao, C. Li, S.-Y. Liu, B. Fang and H. Yang, Z-scheme systems: From fundamental principles to characterization, synthesis, and photocatalytic fuel-conversion applications, *Phys. Rep.*, 2022, **983**, 1–41.
7 S. Feizpoor, S. R. Pouran and A. H. Yangjeh, Recent progress on photocatalytic evolution of hydrogen gas over TiO_{2-x}-based emerging nanostructures, *Mater. Sci. Semicond. Process.*, 2023, **162**, 107444.
8 N. M. Gupta, Factors affecting the efficiency of a water splitting photocatalyst: A perspective, *Renewable Sustainable Energy Rev.*, 2017, **71**, 585–601.
9 D. R. Eddy, M. D. Permana, L. K. Sakti, G. A. N. Sheha, Solihudin, S. Hidayat, T. Takei, N. Kumada and I. Rahayu, Heterophase Polymorph of TiO_2 (Anatase, Rutile, Brookite, TiO_2 (B)) for Efficient Photocatalyst: Fabrication and Activity, *Nanomaterials*, 2023, **13**, 704.
10 J. Joo, S. G. Kwon, T. Yu, M. Cho, J. Lee, J. Yoon and T. Hyeon, Large-Scale Synthesis of TiO_2 Nanorods via Nonhydrolytic Sol–Gel Ester Elimination Reaction and Their Application to Photocatalytic Inactivation of *E. coli*, *J. Phys. Chem. B*, 2005, **109**, 15297–15302.
11 T. Luttrell, S. Halpegamage, S. J. Tao, J. A. Kramer, A. E. Sutter and M. Batzill, Why is anatase a better photocatalyst than rutile? - Model studies on epitaxial TiO_2 films, *Sci. Rep.*, 2014, **4**, 4043.
12 M. Rafique, S. HajraMuneeb, I. Muhammad, U. Muhammad, I. Mohammad, A. A. Waqar and M. Ashraf, Hydrogen Production Using TiO_2-Based Photocatalysts: A Comprehensive Review, *ACS Omega*, 2023, **29**, 25640–25648.
13 M. Batzill, Fundamental aspects of surface engineering of transition metal oxide photocatalysts, *Energy Environm. Sci.*, 2011, **4**, 3275–3286.

14 J. N. Wilson and H. Idriss, Structure sensitivity and photocatalytic reactions of semiconductors. Effect of the last layer atomic arrangement, *J. Am. Chem. Soc.*, 2002, **124**, 11284–11285.
15 M. Xu, Photocatalytic activity of bulk TiO_2 anatase and rutile single crystals using infrared absorption spectroscopy, *Phys. Rev. Lett.*, 2011, **106**, 138302.
16 H. Tang, K. Prasad, R. Sanjines, P. E. Schmid and F. Levy, Electrical and optical properties of TiO_2 anatase thin films, *J. Appl. Phys.*, 1994, **75**, 2042.
17 L. Thulin and J. Guerra, Calculations of strain-modified anatase TiO_2 band structures, *Phys. Rev. B*, 2008, **77**, 195112.
18 J. Joy, J. Mathew and S. C. George, Nanomaterials for photoelectrochemical water splitting-Review, *Int. J. Hydrog. Energy*, 2018, **43**, 4804–4817.
19 P. Kumar, P. Devi, R. Jain, S. M. Shivaprasad, R. K. Sinha, G. Zhou and R. Nötzel, Quantum dot activated, indium gallium nitride on silicon as photoanode for solar hydrogen generation, *Commun. Chem.*, 2019, **2**, 4.
20 T. Le, K. Mawatari, Y. Pihosh, T. Kawazoe, T. Yatsui, M. Ohtsu, M. Tosa and T. Kitamori, Optical near-field induced visible response photoelectrochemical water splitting on nanorod TiO_2, *Appl. Phys. Lett.*, 2011, **99**, 213105.
21 B. Li, Q. Li, B. Gupta, Z. Guan, L. Zhang, M. Zhang and J. Yang, Space-induced charge carriers separation enhances photocatalytic hydrogen evolution on hollow urchin-like TiO_2 nanomaterial, *J. Alloys Compd.*, 2020, **837**, 155547.
22 H. Eidsvåg, S. Bentouba, P. Vajeeston, S. Yohi and D. Velauthapillai, TiO_2 as a Photocatalyst for Water Splitting-An Experimental and Theoretical Review, *Molecules*, 2021, **26**, 1687.
23 Y. Pihosh, I. Turkevych, K. Mawatari, N. Fukuda, R. Ohta, M. Tosa, K. Shimamura, E. G. Villora and T. Kitamori, Ubiquitous element approach to plasmonic enhanced water splitting: the case of $Ti@TiO_2$ core-shell nanostructure, *Nanotechnology*, 2014, **25**, 315402.
24 D. P. Kumara, V. D. Kumarib, M. Karthik, M. Sathishd and M. V. Shankar, Shape dependence structural, optical and photocatalytic properties of TiO_2 nanocrystals for enhanced hydrogen production via glycerol reforming, *Sol. Energy Mater. Sol. Cells*, 2017, **163**, 113–119.
25 N. Murakami, S. Kawakami, T. Tsubotaa and T. Ohno, Dependence of photocatalytic activity on particle size of a shape-controlled anatase titanium (IV) oxide nanocrystal, *J. Mol. Catal. A: Chem.*, 2012, **358**, 106–111.
26 Y. K. Kho, A. Iwase, W. Y. Teoh, L. Mädler, A. Kudo and R. Amal, Photocatalytic H_2 Evolution over TiO_2 Nanoparticles. The Synergistic Effect of Anatase and Rutile, *J. Phys. Chem. C*, 2010, **114**, 2821–2829.
27 H. H. Do, D. L. T. Nguyen, X. C. Nguyen, T. H. Le, T. P. Nguyen, Q. T. Trinh, S. H. Ahn, D. V. N. Vo, S. Y. Kim and Q. V. Le, Recent progress in TiO_2-based photocatalysts for hydrogen evolution reaction: A review, *Arabian J. Chem.*, 2020, **13**, 3653–3671.
28 S. Pokrant, S. Dilger, S. Landsmann and M. Trottmann, Size effects of cocatalysts in photoelectrochemical and photocatalytic water splitting, *Mater. Today Energy.*, 2017, **5**, 158–163.
29 J. Schneider, M. Matsuoka, M. Takeuchi, J. Zhang, Y. Horiuchi, M. Anpo and D. W. Bahnemann, Understanding TiO 2 Photocatalysis: Mechanisms and Materials, *Chem. Rev.*, 2014, **114**, 9919–9986.
30 Y. Wang, L. Li, X. Huang, Q. Li and G. Li, New insights into fluorinated TiO_2 (brookite, anatase and rutile) nanoparticles as efficient photocatalytic redox catalysts, *RSC Adv.*, 2015, **5**, 34302.
31 N. D. Johari, Z. M. Rosli, J. M. Juoi and S. A. Yazid, Comparison on the TiO_2 crystalline phases deposited via dip and spin coating using green sol–gel route, *J. Mater. Res. Technol.*, 2019, **8**, 2350–2358.
32 W. Hu, L. Li, W. Tong and G. Li, Supersaturated Spontaneous Nucleation to TiO_2 Microspheres: Synthesis and Giant Dielectric Performance, *Chem. Commun.*, 2010, **46**, 3113–3115.
33 S. Sadhu, P. Gupta and P. Poddar, Physical Mechanism Behind Enhanced Photoelectrochemical and Photocatalytic Properties of Superhydrophilic Assemblies of 3D-TiO_2 Microspheres with Arrays of Oriented, Single-Crystalline TiO_2 Nanowires as Building Blocks Deposited on Fluorine-Doped Tin Oxide, *ACS Appl. Mater. Interfaces*, 2017, **9**, 11202–11211.
34 K. S. Kim, J. K. Kim and W. S. Kim, Influence of reaction conditions on sol-precipitation process producing silicon oxide particles, *Ceram. Int.*, 2002, **28**, 187–194.
35 A. E. Danks, S. R. Hall and Z. Schnepp, The evolution of 'sol–gel' chemistry as a technique for materials synthesis, *Mater. Horiz.*, 2016, **3**, 91.
36 C. T. Dinh, T. D. Nguyen, F. Kleitz and T. O. Do, Shape-Controlled Synthesis of Highly Crystalline Titania Nanocrystals, *ACS Nano*, 2009, **3**, 3737–3743.
37 S. Sadhu and P. Poddar, Template-Free Fabrication of Highly Oriented Single-Crystalline 1D Rutile TiO_2-MWCNT Composite for Enhanced Photoelectrochemical Activity, *J. Phys. Chem. C*, 2014, **118**, 19363–19373.
38 E. M. Huseynov and E. A. Huseynova, Infrared spectroscopy of nanocrystalline anatase (TiO_2) particles under neutron irradiation, *Opt. Mater.*, 2023, **144**, 14351.
39 T. Hisatomi, J. Kubota and K. Domen, Recent advances in semiconductors for photocatalytic and photoelectrochemical water splitting, *Chem. Soc. Rev.*, 2014, **43**, 7520.
40 R. Shwetharani, M. Sakar, C. A. N. Fernando and V. B. R. Geetha Balakrishna, Recent advances and strategies to tailor the energy levels, active sites and electron mobility in titania and its doped/composite analogues for hydrogen evolution in sunlight, *Catal. Sci. Technol.*, 2019, **9**, 12.
41 D. O. Scanlon, C. W. Dunnill, J. Buckeridge, S. A. Shevlin, A. J. Logsdail, S. Woodley, M. Richard, C. Catlow, A. Powell, M. J. Palgrave, R. G. Parkin, I. P. Watson, G. W. Keal, T. W. Sherwood, P. Walsh and A. Sokol, Band alignment of rutile and anatase TiO_2, *Nat. Mater.*, 2013, **12**, 798–801.

42 K. Zakrzewska, Nonstoichiometry in TiO_{2-y} Studied by Ion Beam Methods and Photoelectron Spectroscopy, *Adv. Mater. Sci. Eng.*, 2012, **826873**, 1–13.
43 B. Dong, J. Cui, Y. Qi and F. Zhang, Nanostructure Engineering and Modulation of (Oxy)Nitrides for Application in Visible-Light-Driven Water Splitting, *Adv. Mater.*, 2021, **33**, 2004697.
44 B. Gupta, A. Aziz, S. Sundriyal, V. Shrivastav, A. A. Melvin, M. Holdynski and W. Nogala, *Sci. Rep.*, 2023, **13**, 5019.
45 S. F. Shaikh, R. S. Mane, B. K. Min, Y. J. Hwang and O. S. Joo, D-sorbitol-induced phase control of TiO_2 nanoparticles and its application for dye-sensitized solar cells, *Sci. Rep.*, 2015, **6**, 20103.
46 O. Fontelles-Carceller, M. J. Muñoz-Batista, E. Rodríguez-Castellón, J. C. Conesa, M. Fernández-García and A. Kubacka, Measuring and interpreting quantum efficiency for hydrogen photo-production using Pt-titania catalysts, *J. Catal.*, 2017, **347**, 157–169.
47 S. E. Salas, B. S. Rosales and H. de Lasa, Quantum yield with platinum modified TiO_2 photocatalyst for hydrogen production, *Appl. Catal., B*, 2013, **140**, 523–536.
48 B. Wang, D. H. C. Wan, A. T. F. Cheung, D. Y. C. Leung, X. Y. Lu and M. K. H. Leung, Green hydrogen production by solar photocatalysis using Pt-TiO_2 nanosheets with reactive facets, *HKIE Trans.*, 2021, **28**, 75–81.
49 E. P. Melian, C. R. Lopez, A. O. Mendez, O. G. Dıaz, M. N. Suarez, J. M. D Rodrıguez, J. A. Navıo and D. F. Hevia, Hydrogen production using Pt-loaded TiO_2 photocatalyst, *Int. J. Hydrogen Energy*, 2013, **38**, 11737–11748.